Multifractal scaling of flux penetration in the Iron-based Superconductor $Ba(Fe_{0.925}Co_{0.075})_2As_2$

Mathieu Grisolia and Cornelis J. van der Beek
Laboratoire des Solides Irradiés, CNRS UMR 7642 & CEA-DSM-IRAMIS, Ecole Polytechnique, F91128 Palaiseau cedex, France

Yanina Fasano
Laboratorio de Bajas Temperaturas, Centro Atómico Bariloche & Instituto Balseiro, Avenida Bustillo 9500, 8400 Bariloche, Argentina

Anne Forget, Dorothée Colson
Service de Physique de l'Etat Condensé, Orme des Merisiers, CEA Saclay (CNRS URA 2464), 91191 Gif sur Yvette cedex, France
(Dated: January 17, 2013)

The penetration of magnetic flux fronts in the optimally doped iron based superconductor $Ba(Fe_{0.925}Co_{0.075})_2As_2$ is studied by means of magneto-optic imaging and Bitter decoration. The higher-order analysis of roughening and growth of the magnetic flux front reveals anomalous scaling properties, indicative of non-Gaussian correlations of the disorder potential. While higher-order spatial correlation functions reveal multi-fractal behavior for the roughening, the usual Kardar-Parisi-Zhang growth exponent is found. Both exponents are found to be independent of temperature. The scaling behavior is manifestly different from other modes of flux penetration, such as that mediated by avalanches, suggesting that multi-scaling is a powerful tool for the characterization of roughened interfaces. We propose a scenario for vortex penetration based on 2D percolation and cluster aggregation in an inhomogeneously disordered superconductor.

PACS numbers: 74.25.Wx,68.35.Ct,64.60.al,74.25.Op

I. INTRODUCTION

Vortex line pinning and the ensuing irreversible magnetic properties of type-II superconductors have been studied for many years. These are usually described in terms of the Bean model and its generalizations.[1–7] While the Bean model accounts for global magnetic properties such as magnetization hysteresis loops and macroscopic flux distributions, it does not describe the local fluctuations of vortex densities $n_v = \langle \mathbf{B} \rangle_{\lambda_L}/\Phi_0$ in time and space,[8,9] nor the roughness of the magnetic flux penetration front. Here $\langle \mathbf{B} \rangle_{\lambda_L}$ is the coarse-grained flux density, averaged over a distance of the order of the penetration depth λ_L, and $\Phi_0 = h/2e$ is the flux quantum. Due to the wide range of phenomena in which front growth and roughening occur, such as fluid flow in porous media,[10] propagation of the ignition front in burning paper,[8,11] or the advancement of a rice pile,[12–16] and the many analogies between these different phenomena, the subject has raised a huge amount of interest over the last 25 years.

The analysis of local variations δh of the magnetic flux front height $h(x)$ is commonly performed using the height-height correlation function[17]

$$C^2(x,t) = \left\langle \left[\delta h(x',\tau) - \delta h(x'+x,\tau+t)\right]^2 \right\rangle_{x',\tau} \quad (1)$$

where $\delta h(x,t) = h(x,t) - \langle h(x,t) \rangle_x$ corresponds to the local deviation from the average front position, and $\langle ... \rangle_{x',\tau}$ denotes averaging over the spatial coordinate as well as time. In our case, time steps correspond to increments in the applied magnetic field $\mu_0 H_a$.

The quantity (1) enables one to simultaneously determine both the roughness exponent α and the growth exponent β by fitting the respective evolution

$$C(x,0) \propto x^{\alpha} \qquad (x \ll l_{sat}) \quad (2)$$
$$C(0,t) \propto t^{\beta} \qquad (t \ll t_{sat}). \quad (3)$$

The saturation length l_{sat} is the distance over which the front shape influences the height at a given site. The saturation time t_{sat} is the time scale beyond which the influence of the previous evolution of the front is lost.

Theoretical models predict different scaling properties of roughened interfaces, depending on its (non)equilibrium state and the type of disorder to which the interface is subjected. Usually, one has a competition between two antagonistic mechanisms, such as the elasticity of the interface, which tends to smooth it, and its interaction with a disorder potential, responsible for roughening. A powerful theoretical approach to kinetic roughening is represented by the so-called Kardar-Parisi-Zhang (KPZ) model[18] which describes the temporal evolution of the height variable $h(x,t)$,

$$\frac{\partial h}{\partial t} = \nu \nabla^2 h + \mu (\nabla h)^2 + \eta(x,h;t) + F. \quad (4)$$

Here ν is an effective surface tension; μ quantifies the importance of lateral growth and vanishes for zero velocity, and F is an external force. The disorder term $\eta(x,y;t)$ has a Gaussian distribution with zero mean,

and $\langle \eta(x,t)\eta(x',t')\rangle = 2D\delta(x-x')\delta(t-t')$. Eq. (4) well describes diverse phenomena of kinetic roughening such as ballistic deposition or Eden models[18] but also the advancement of flux fronts in type II superconductors.[8] This is due to the growth front height being perpendicular to the front itself, since the Lorentz force $F_L = \mathbf{j} \times \mathbf{B}$. The KPZ model predicts well-defined roughness and growth exponents, $\alpha = \frac{1}{2}$ and $\beta = \frac{1}{3}$. In parallel, however, a wide variety of exponents has been reported in other systems, including wetting, imbibition, percolation, bacteria invasion, and so forth.[19,20] Among different approaches to account for such phenomena, Barabási *et al.* proposed to apply the concept of multifractality to interface roughness.[21–23] Multifractality has been associated with a power-law distribution of the noise amplitude η, that accounts for rare events in the roughening or growing process. It is also relevant for the roughening of linear polymers on percolation clusters.[24–26] Alternatively, a multifractal formalism may be useful if different length scales compete in the growth process, or if depinning occurs at preferential sites. In those cases, rare events such as avalanches may drive the kinetic properties.[27,28]

Regarding to magnetic flux fronts in superconductors, Surdeanu *et al*[8] were the first to study different models to account for the roughening of the interface between the mixed state and Meissner phase in thin–film cuprate superconductors. The authors[8] distinguished two regimes in roughening and growth: a short–range interaction regime was well-described by the Directed Percolation Depinning (DPD) model,[20] while the long–range regime is described by a usual 1+1-KPZ equation. Through the mapping of front progression through a quenched disorder potential on the problem of percolation, the DPD model predicts values $\alpha = 0.63$ and $\beta = 0.65$. On the other hand, Eq. (4) explicitly includes temporal fluctuations of the disorder. DPD-like behavior was also reported for flux penetration in Nb thin films on Si-substrates, over a narrow temperature window between smooth flux fronts at high T, and an avalanche-dominated regime at low T.[30] The authors[30] noted that the observed scaling might be due to KPZ behavior in the presence of spatially correlated (non-Gaussian) disorder.

Below we characterize the penetrating flux front in single crystals of the optimally–doped iron-based superconductor $Ba(Fe_{0.925}Co_{0.075})_2As_2$ using the recently developed multi-scaling approach. The roughened front shows self-affine behavior, indicating non-Gaussian correlations of the disorder potential. Strikingly, the growth exponent is in agreement with the KPZ model. The multiscaling of the front roughness is clearly different from that produced by either avalanche dynamics in Nb thin films[31–33] or depinning of a ferro-electric domain wall from a mixture of strong and weak pinning sites.[34]

We propose a tentative interpretation based on the findings of Ref. 35 for $Ba(Fe_{1-x}Co_x)_2As_2$. That work reports that nanometer-scale inhomogeneity of the superconducting properties is at the origin of the lack of even intermediate–range vortex positional order, and of the significant vortex density fluctuations observed on field cooling.[35] Spatial variations of superconducting parameters such as the critical temperature, T_c, or the superfluid density, n_s, would result in a random network of more-or-less favorable sites, suggesting the analogy with a percolation cluster. The difference in multi-scaling of the roughness and growth exponents suggests the percolation and aggregation of different clusters (front sections) with different fractal dimension.

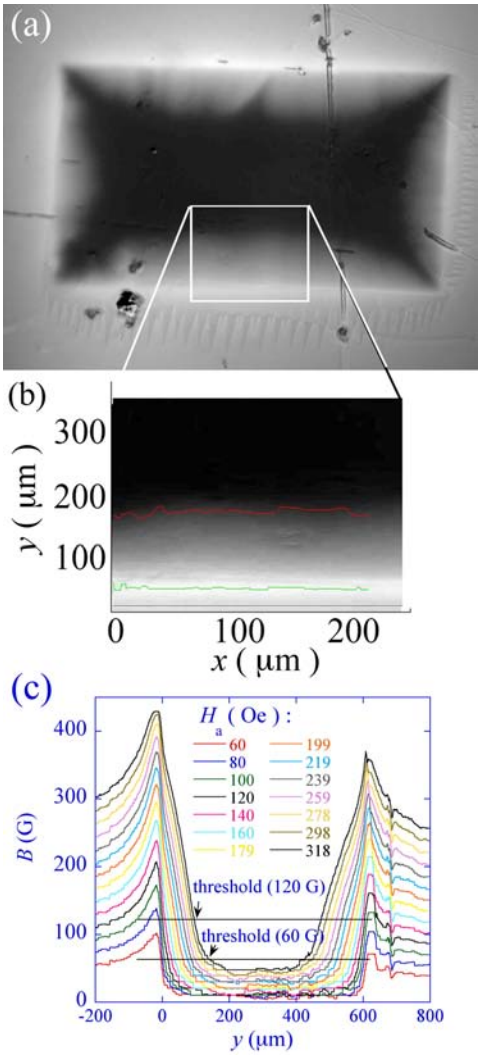

FIG. 1: (a) Magneto-optical image of flux-penetration into $Ba(Fe_{0.925}Co_{0.075})_2As_2$ crystal # 1, taken at $H_a = 404$ Oe after zero field cooling to 10 K. The zoom in (b) shows the part that is used in the analysis. The red line indicates the flux front, determined as the induction threshold $B = 120$ G above the luminous intensity value corresponding to the Meissner state. The green line shows the crystal edge. (c) Average Bean–like flux density profile across the crystal width in the y-direction (perpendicular to the long sample edge). Flux density thresholds of 60 and 120 G are indicated.

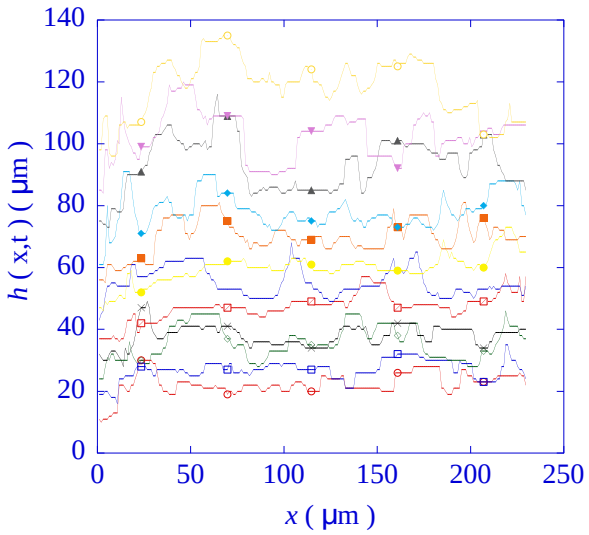

FIG. 2: Flux fronts determined in crystal # 1 at 10 K, using an induction threshold of 120 G. The value of the external applied field ranges from 163 (bottom) to 383 Oe (top).

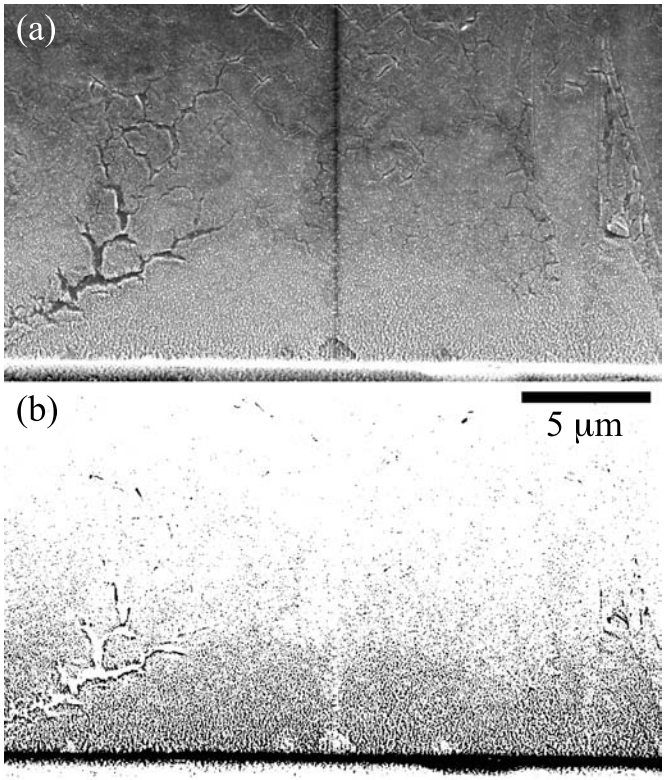

FIG. 3: (a) Bitter decoration image of flux penetration into crystal # 1, at an applied field $H_a = 80$ Oe (at which the mean distance between vortex lines $a_0 = 0.54$ μm). The image depicts the untreated Scanning Electron Micrograph of a 40 μm–long section of the region of the sample shown in Fig. 1b. The crystal edge corresponds to the bright line at the bottom. Individual vortices appear as white dots. (b) *ibid.* An intensity thresholding has been applied to the negative image of (a) in order to bring out the vortex positions as well as the flux front. The corrugation of the magnetic flux penetration front in the centre of the image is clearly observed.

II. EXPERIMENTAL DETAILS

Optimally–doped $Ba(Fe_{0.925}Co_{0.075})_2As_2$ single crystals, with critical temperature $T_c = 24.5$ K, were grown using the self-flux method, as described in Ref. 36. Crystal # 1 has a length of 994 μm, a width of 571 μm, and a thickness of 32 μm. Its critical current density (at $T = 10$ K) is $j_c = 2.4\times10^8 \mathrm{Am}^{-2}$; crystal # 2 has a length of 835 μm, a width of 733 μm, a thickness of 27 μm, and $j_c(10\,\mathrm{K}) = 3.1\times10^8 \mathrm{Am}^{-2}$. The penetration of magnetic flux into the selected crystals was first visualized by the magneto-optical imaging (MOI) method.[37,38] A ferromagnetic garnet indicator film with in-plane anisotropy is placed on top of the sample. A non-zero perpendicular component of the magnetic induction B induces an out-of-plane rotation of the magnetization, and, thereby, a Faraday rotation of the polarization of light traversing garnet. An Al mirror evaporated on the hind side of the garnet reflects the impinging light, which is then observed using a polarized light microscope with nearly crossed polarizer and analyzer. Regions with nonzero B then show up as bright when observed through the analyzer. Fig. 1(a) shows the penetration of magnetic flux into $Ba(Fe_{0.925}Co_{0.075})_2As_2$ crystal # 1, the rectangular outline of which is clearly seen. We shall be interested in the flux front within the sample, between peripheral bright regions of non-zero B, and the dark central region of $B = 0$. This front corresponds to the interface between the mixed state, in which the superconductor is penetrated by vortex lines, and the Meissner phase of excluded magnetic flux. In order to avoid bias and distortions induced by the effect of the crystal corners on the shape of the flux front, we have studied the penetration near the center of the crystal edges only. At all measurement temperatures, the temperature stability was better than 10 mK; the external field was increased in 20 Oe steps in order to monitor the flux front progression.

The MO images are converted to maps of the magnetic induction by calibrating the luminous intensity with respect to the applied field.[38] Next, the position of the flux front is determined from a given threshold level of the magnetic induction on the flux profiles. Using non-zero threshold value avoids uncontrolled variations between experiments due to the specific luminosity and polarization conditions under which images are acquired. All in all, 17 different threshold values between 40 and 200 G were used. The minimum threshold value that could be used for all applied field values was $B = 120$ G. We define the height $h(x)$ of the flux front as the distance between the position at which the magnetic induction is maximum

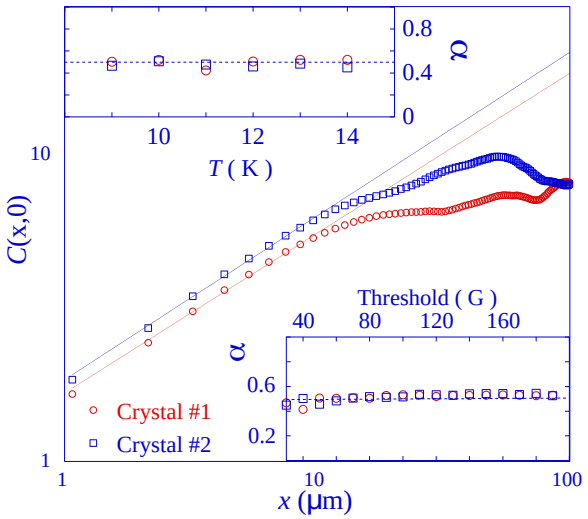

FIG. 4: Main panel: Two-point correlation function of the penetrating flux front, *i.e.* the square-root of the quantity of Eq. (1), calculated for the flux front at 10 K in crystals # 1(red ○) and # 2 (blue □). The roughness exponent is, by definition, the slope of the linear (solid lines) regime of $C(x,0)$ in a log-log plot. For crystal # 2, this value is in perfect agreement with the KPZ model, *i.e.* $\alpha = 0.50$. Upper inset: Temperature independence of the roughness exponent. Lower inset: Independence of α as a function of the threshold value of the induction threshold, as this ranges from 40 to 200 G. In both insets, $\alpha \approx 0.5$ (dashed lines)

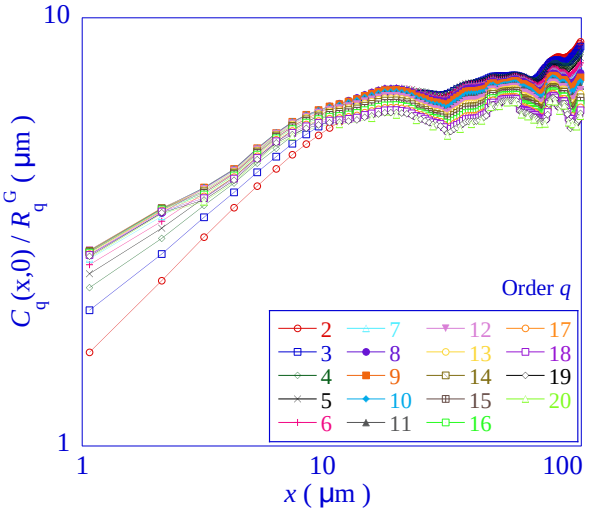

FIG. 5: Higher order spatial correlation function $C_q(x,t)$, normalized by the Gaussian ratios R_q^G,[23,34] with q varying from 2 to 20, as measured on the penetrating flux front in $Ba(Fe_{0.925}Co_{0.075})_2As_2$ crystal # 2 at $T = 10$ K. The slope depends continuously on q and presents nontrivial scaling. The behavior is therefore multifractal. The same behavior is found for sample #1.

at the sample boundary, and the position of the intensity threshold, along a 1 pixel-wide strip perpendicular to the sample boundary. Such a definition eliminates the effect of possible shifts in the luminous intensity due to overexposure of certain strips in the camera. An example of the progression of the flux front so determined in crystal # 1 is shown in Fig. 2. In order to evaluate the correlation function (1), we subtract the mean position of the flux front $\langle h(t)\rangle_x$, averaged over the 250 μm–wide central section of the crystal on which the analysis is performed.

In order to observe the flux front morphology on a finer scale, and, notably, to investigate the reality of coalescing clusters, Bitter decoration[39] was performed on the same crystals after zero-field cooling to 4.2 K and the application of a field of 80 Oe. Typical results (on crystal #1) are shown in Fig. 3. The image shows individual vortex lines as these enter the crystal from the lower edge. Note that the intervortex distance near the edge $a_0 \equiv (\Phi_0/\langle B\rangle_{\lambda_L})^{1/2} = 0.54$ μm. Similar images were obtained along all four crystal edges.

III. ANALYSIS OF THE FLUX FRONT

The main panel of Fig. 4 shows the spatial correlation function $C(x,0)$, describing flux penetration from the lower edge of crystal # 1 at $T = 10$ K. The value of the roughness exponent determined from the logarithmic slope of $C(x,0)$ versus x is very close to the value derived in the KPZ model, $\alpha = \frac{1}{2}$.[17] In this respect, our data are similar to those of Ref. 8. The constant value of $C(x,0)$ for separations larger than $x_{sat} \approx 10$ μm indicates that beyond this length scale, deformations of the flux front are independent. The value of x_{sat} is possibly related to the (similar) dimensions of independently penetrating vortex clusters, to be discussed below.

In order to ascertain the robustness of these results, we have checked for temperature and vortex density dependence. At sufficiently low flux densities the distance a_0 between vortex lines exceeds $\lambda_L(T)$. Since λ_L increases with T, the interaction between vortices also increases with T within this B-range (for a fixed vortex density). On the contrary, at higher vortex densities, $a_0 < \lambda_L(T)$, and the repulsive interaction decreases with T. Hence, vortex lines are not sensitive to the same length scales of disorder for different T and B, so that, for non-trivial correlations of the disorder, a continuous evolution of $\alpha(T,B)$ might be expected. However, the upper inset to Fig. 4 clearly shows that the roughness exponent does not depend on temperature.

Investigating the dependence of the roughness exponent on vortex density corresponds to probing the dependence on the threshold value. The independence of α on threshold, displayed in the lower inset to Fig. 4, underscores the lack of dependence on temperature, since both imply that the front roughness does not depend on

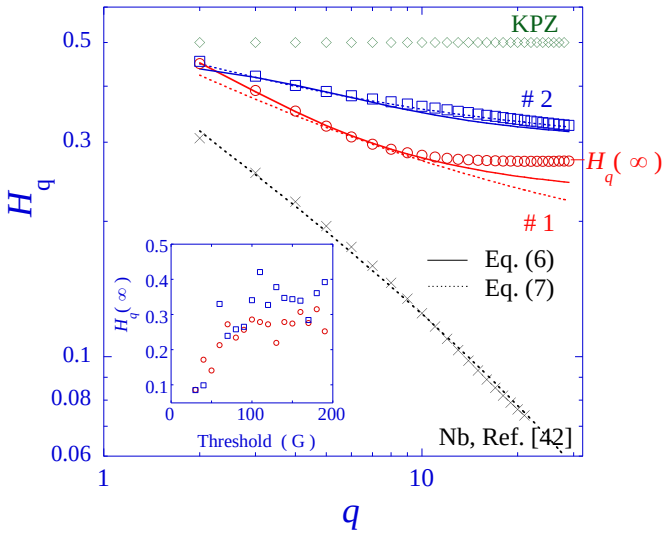

FIG. 6: The exponent H_q as a function of the order q for the magnetic flux front in $Ba(Fe_{0.925}Co_{0.075})_2As_2$ crystals # 1 (red ○) and # 2 (blue □), evaluated for a given threshold of $B = 120$ G. For comparison, $H_q = \frac{1}{2}$ for the KPZ model is also shown (green ◇), as is the result of the analysis of the flux penetration observed at 6 K in the superconducting Nb films of Refs. 32 and 33 (×). The decay of H_q measured on the superconducting samples is monotonous, without any inflection. For the $Ba(Fe_{0.925}Co_{0.075})_2As_2$ crystals, H_q saturates at a lower, resolution–limited bound $H_q(\infty)$, the evolution of which as function of the flux-density threshold used to determine the flux–front is shown in the Inset. H_q compares well with Eq. (6), with $(b_1, b_2) = (0.2, 0.73)$ and $(0.4, 0.66)$ for crystals 1 and 2, respectively. A comparison with Eq. (7) (dotted lines) yields parameters sets $(a, b, c) = (2, 26.3, 0.15)$, $(1.2, 24, 0.28)$, and $(2.1, 17.6, -0.03)$ for crystals 1, 2, and the Nb–film of Refs. 32 and 33, respectively.

the strength of the vortex interaction. A tentative explanation is suggested by Ref. 35: that vortices in the $Ba(Fe_{1-x},Co_x)_2As_2$ crystals are sensitive to disorder on widely different length scales, so that, at any stage of flux penetration, they always find an optimal pinning site.

We now turn to the multiscaling analysis of the data. The method[23,25,34] relies on the computation of the higher-order two–point correlation function

$$C_q(x,t) = \langle [\delta h(x',\tau) - \delta h\,(x'+x, \tau+t)]^q \rangle_{x',\tau}{}^{1/q}. \quad (5)$$

Following previous work,[21] C_q should scale as $C_q(x,0) \propto x^{H_q}$, with H_q the generalized Hurst exponent. A nontrivial q-dependent scaling is the hallmark of a non-Gaussian probability density function (PDF) of the disorder, leading to a self-affine (but not self-similar) interface.[21] More generally, it may indicate multifractal behavior, *i.e* the geometry of the interface is not simply fractal but implies many different geometries of many different fractal dimensions.[40] On the contrary, a constant $H_q = \alpha = 0.5$ is representative of KPZ behavior and of an interface with a Gaussian PDF (see Ref. 22 and Fig. 6). Figure 5 shows the higher order two-point correlation functions evaluated on the flux fronts in crystal # 1, normalized by the factors $R_q^G \equiv C_q^G(x,0)/C_2^G(x,0)$,[23,34] with q ranging from 2 to 20. Here, the correlation functions $C_q^G(x,t)$ are those that would be obtained for an interface with a Gaussian PDF of the local displacements.[23,34] Figure 6 shows the behavior of the exponent H_q as a function of q for the magnetic flux fronts in our $Ba(Fe_{0.925}Co_{0.075})_2As_2$ crystals. The saturation of H_q to a sample–dependent value $H_q(\infty)$ at large q is the result of the resolution limit in our experiment. From Figs. 5 and the exponent H_q rendered in 6, it is clear that, for small x, the scaling with length depends on the order q in a non-trivial manner. Similar $H_q(q)$-dependences were obtained for the front on the opposite side of the crystal, and for flux fronts in the other investigated $Ba(Fe_{0.925}Co_{0.075})_2As_2$ crystals. More importantly, the same multiscaling is observed even when a subsection of the investigated front is considered.

The q-dependence of the Hurst exponent describing the flux fronts in $Ba(Fe_{0.925}Co_{0.075})_2As_2$ is remarkably well-rendered by the simple toy model used in Ref. 21 to prove the relevance of multi-scaling for the description of self-affine fractal interfaces,[21]

$$H_q = \frac{\ln\left[\left(b_1^q + b_2^q\right)/2\right]}{q \ln \frac{1}{4}}. \quad (6)$$

Here b_1 and b_2 are the scaling parameters characterizing the self-affine interface structure parallel and perpendicular to the growth direction, such as these are used in Ref. 21 for the construction of a model interface. The experimental values, $(b_1, b_2) = (0.2, 0.73)$ and $(0.4, 0.66)$ for crystals 1 and 2, respectively, clearly demonstrate the irrelevance of a Gaussian PDF for the transverse excursions of the flux front in $Ba(Fe_{0.925}Co_{0.075})_2As_2$, which would yield a constant roughness exponent $\frac{1}{2}$. A self-similar interface with Gaussian PDF can be generated in the toy model[21] by $b_1 = b_2 = 0.5$.

We have also evaluated multiscaling of growth of the flux front height. Figure 7 shows that the temporal correlation functions $C_q(0,t) = C_q(0, H_a/\dot{H}_a)$ are parallel for all q, and scale with the Gaussian factors R_q^G. The temporal correlation functions obey the same power-law behavior, $C_q(0,t) \sim t^{0.33}$. We consider this value to be in agreement with $\beta = \frac{1}{3}$ from KPZ theory. We thus find, surprisingly, that the evolution of the flux fronts in the $Ba(Fe_{0.925}Co_{0.075})_2As_2$ crystals corresponds to the diffusive growth of a multi-fractal structure.

IV. DISCUSSION

A number of propositions have been made to explain the origin of multifractality and multiscaling. A non-Gaussian, *e.g.* power–law, PDF underlying the disorder

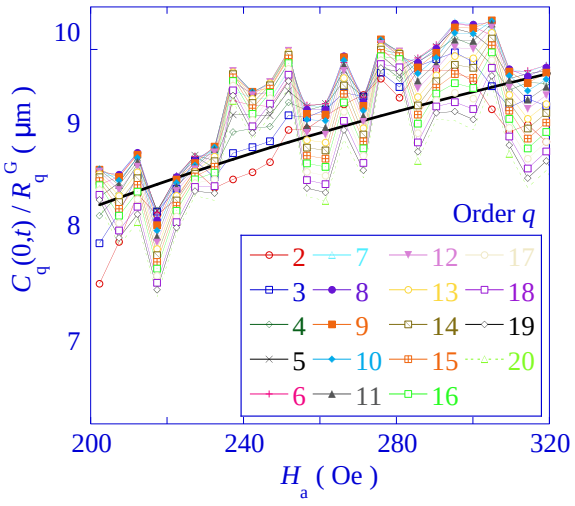

FIG. 7: Higher-order two-point correlation function as function of the temporal evolution of the magnetic flux front in $Ba(Fe_{0.925}Co_{0.075})_2As_2$ crystal # 1, at $T = 11$ K. Data or normalized using the Gaussian factors R_q^G,[23,34] and are represented with the temporal variable on the abscissa expressed as the value of the externally applied magnetic field. For the establishment of these curves, only the field values between 197 and 393 G were taken into account – for lower fields, flux does not penetrate, for higher fields, complete penetration is achieved. The $C_q(0,t)$ show the same behavior for all q, ranging from $q = $ to $q = 20$, and scale with the R_q^G–values. The data compare well with the KPZ prediction, $C_q(0,t) \sim t^{1/3}$(black line).

term η,[29] was introduced for the description of percolative imbibition of a fluid by paper. The link between penetrating flux fronts and the porous medium equation for the imbibition by fluids was previously remarked in Refs. 8 and 41. However, the porous medium equation as such, as analyzed in Ref. 41, does not lead to (multi–)fractal behavior.

A second explanation for anomalous scaling in roughening processes is the occurrence of avalanches.[13,14,28,42,43] The numerical work of Bassler *et al.* showed the possible multi-fractal character of braided vortex trajectories resulting from avalanches in a strongly pinning superconductor.[43] The effect of local temperature variations on the nucleation and propagation of dendritic vortex avalanches was investigated experimentally by Welling *et al.*,[31,32] who studied thin superconducting Nb films deposited on sapphire substrates of various orientations. The authors[31,32] found that, in 500 nm-thick Nb deposited on A–plane sapphire, flux penetration at low temperature ($T < 6$ K) takes place via huge compact avalanches, while at $T > 6$ K the flux penetration is more regular, yielding continuous flux fronts. The latter bear a certain resemblance to those observed in the present work. Numerical work by Aranson *et al.*[33] suggests that avalanches in defect-free films occur at periodic locations, while avalanches in films with edge defects are initiated at these imperfections. With this in mind, it was suggested[33] that both avalanche–like and more regular flux penetration in Nb/A–plane sapphire is initiated by edge defects. In order to ascertain whether the roughened flux fronts in $Ba(Fe_{0.925}Co_{0.075})_2$ have a similar origin, we have analyzed the structure of the continuous flux fronts ($T > 6$ K) reported in movie 8 of Ref. 44, which shows flux penetration such as that reproduced in Fig. 8(a). To perform this analysis, we considered a threshold of 10 % of the applied field. The analysis of the correlation function (5) shows that the flux fronts in this Nb thin film show multi-scaling behavior (Nb data in Fig. 6). The Hurst exponent starts off with a lower value $H_2 = 0.3$, and decreases as a near power–law to zero as q increases. However, contrary to our results on $Ba(Fe_{0.925}Co_{0.075})_2As_2$, this curve is not satisfactorily described by Eq. (6). Moreover, the high-temperature flux penetration as shown in Ref. 32, 33 , and 44 *does* obey multi-scaling during growth, see Fig. 8(b). An explanation for this is that even temperatures higher than 6 K, the "regular" flux penetration in Nb thin films would be the result of the superposition of many

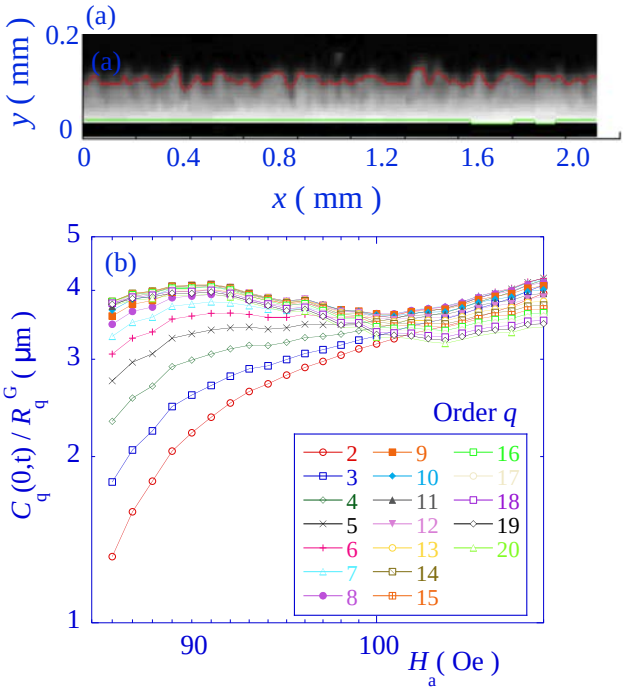

FIG. 8: (a) Flux front in 500 nm-thick Nb thin film, deposited on A-plane sapphire, at $T = 6$ K and $H_a = 1.5$Oe (data taken from Ref. 44). (b) Multi-scaling analysis of the growth behavior of such a flux-front. Contrary to the case of $Ba(Fe_{0.925}Co_{0.075})_2As_2$, $C_q(0,t)$ has a q-dependent temporal behavior also. The q–dependent correlation function fans out at small times, *i.e.* small applied fields, but shows q-independent behavior at large times.

avalanches. The observed q-dependence would then be induced by the avalanche size distribution, which follows a power–law distribution in space and time.

Clearly, the roughening and growth of the flux front observed in the $Ba(Fe_{0.925}Co_{0.075})_2As_2$ crystals is dissimilar from the superposition of thermo-magnetic avalanche-like instabilities as observed in the case of Nb thin films. A more pertinent analogy may be that suggested by the analysis of roughened ferro-electric domain walls.[34] In that particular work, "mono-affine" scaling of the domain-walls, with a Gaussian PDF of its local transverse displacements, was found on small length scales, both in numerical simulations as in actual experiments on $Pb(Zr_{0.2}Ti_{0.8})O_3$. Such a mono-affine behavior corresponds to so-called "weak-collective pinning", in which the domain wall is only pinned by the fluctuations in the pin density. Analysis on larger length scales showed "multi-affine scaling" described by a non-trivial hierarchy of higher-order scaling exponents. The crossover length scale in the study[34] was given by that on which rare events in the form of strongly pinning defects such as dislocations occur. Translated to our experiments, this would correspond to the mono-affine (KPZ-like) growth of individual front sections emanating from specific sections of the boundary of the superconducting crystal, separated by sections from which flux penetration is less likely. Such edge inhomogeneity might then be interpreted in terms of the local variation of superconducting properties[35] and / or geometrical irregularities at the crystal edges. However, in our analysis, multiscaling is the same irrespective of considering the entire length of the flux front (see Fig. 1(b)) or a subsection thereof.

A third possibility is the growth and coalescence of front sections with different fractal geometry, arising from different disorder realizations in distinct parts of the $Ba(Fe_{0.925}Co_{0.075})_2As_2$ crystals. Such heterogeneity may be expected, *e.g.*, from the analysis of highly disordered vortex ensembles observed using Bitter decoration.[35] The interaction energy–distribution of these ensembles could be understood only if one admits to the presence of substantial spatial heterogeneity of the superconducting parameters, on the scale of 10 – 100 nm. Front sections with different roughness characteristics would then show diffusive growth, according to the KPZ description, but form an anomalously roughened front upon coalescence. Coalescence was considered in the numerical study of linear polymers on percolation clusters by Blavatskaa and Janke.[25] They proposed that multiscaling could arise from the merger of two fractal structures of different dimensions, keeping their underlying geometry in the process.[25] Once a cluster is formed, its temporal roughening is characterized by a certain growth exponent; the cluster retains the same geometry and dimension during growth. This behavior could account for both the observed temporal monoscaling growth behavior and the multifractal roughening upon the collision of two roughened structures. Indeed, Fig. 3 shows evidence for percolative penetration of vortices at the very interface of the mixed state and the Meissner state in $Ba(Fe_{0.925}Co_{0.075})_2As_2$. Vortex lines are seen to penetrate the crystal in an irregular fashion, the flux front on the μm–scale featuring peninsula–like protrusions separated by vortex–free areas. These features then coalesce to generate a continuous front.

A description of the non-trivial $H_q\,(q)$-dependence is suggested the results of Duplantier for the case of percolation in two dimensions, both for random and self-avoiding walks.[40] The q–dependence of the exponent $\alpha(q)$ describing the metric of the harmonic measure of a two–dimensional near-critical percolation cluster is given by

$$\alpha(q) = c + \frac{a}{\sqrt{bq+1}}, \tag{7}$$

with $a = \frac{5}{2}$, $b = 24$, and $c = \frac{1}{2}$ [Eq. (5) of Ref. 40]. The harmonic measure of a percolation cluster is characterized by a lower dimension than the cluster itself, due to the inaccessibility of sites situated on deep "fjords" on the latter. Aggregation at certain sites on the percolation cluster would correspond to the growth of the flux front at specific locations due to the arrival of a vortex line. Eq. 7 very well describes the experimental $H_q(q)$–dependence of Fig. 6, including that for the flux front in Nb thin films, for very similar parameter values. This would imply that the flux-front in heterogeneous type-II superconductors can be described as the hull of a near-critical percolation network.

V. SUMMARY AND CONCLUSIONS

We have measured and analyzed magnetic flux-penetration fronts in single crystals of the optimally–doped iron based superconductor $Ba(Fe_{0.925}Co_{0.075})_2As_2$, over a wide range of temperatures. Analysis reveals multi-scaling of the higher–order two-point spatial correlation functions of the roughened flux front. This implies that the roughness of the front cannot be described by simple diffusive behavior, that is, by a disorder with a Gaussian probability density function. By implication, the multi-scaling approach is a powerful tool to distinguish between the different properties at the origin of interface roughening. Scaling of the flux-front roughness does not depend on temperature or the induction threshold used to define the front position, nor on macroscopic defects that may exist in particular samples. In contrast, a regular KPZ-like growth of the flux-front is found, excluding avalanche–like behavior as being at the origin of the front roughening. We propose an interpretation of our results in terms of multi–fractal roughening due to the aggregation of vortex clusters with various fractal dimensions. Such clusters could in fact be identified using Bitter decoration, which reveals the structure of the flux front on the scale of individual vortex lines. Once the macro cluster is formed, the front develops in time (*i.e.* with increasing magnetic field) with a classical

KPZ exponent, whose universality class includes DPD (directed percolation depinning).[19,20] We show that this unusual roughening is properly described by a theory for the harmonic measure of a two-dimensional percolation hull.[40] Our results underscore the analogy between percolation in porous media and vortex penetration in inhomogeneous superconductors.

Acknowledgements

This work was partially funded by the grant "MagCorPnic" of the Réseau Thématique de Recherche Avancée "Triangle de la Physique" du Plateau de Saclay, by the Agence Nationale de la Recherche grant "PNICTIDES", and by the support of the ECOS-Sud-MINCyT France-Argentina bilateral program, Grant No. A09E03. Work done in Bariloche was partially funded by PICT 2007-00890 and PICT 2008-294.

[1] C.P. Bean, Phys. Rev. Lett. **8**, 250 (1962).
[2] E. Zeldov, J.R. Clem, M. McElfresh, and M. Darwin, Phys. Rev. B **49**, 9802 (1994).
[3] Ernst Helmut Brandt, Phys. Rev. B **54**, 4246 (1996).
[4] Ernst Helmut Brandt, Phys. Rev. B **58**, 6506 (1998).
[5] Ernst Helmut Brandt, Phys. Rev. B **58**, 6523 (1998).
[6] Grigorii P. Mikitik and Ernst Helmut Brandt, Phys. Rev. B **62**, 6800 (2000).
[7] Grigorii P. Mikitik and Ernst Helmut Brandt, Phys. Rev. B **62**, 6812 (2000).
[8] R. Surdeanu, R. J. Wijngaarden, E. Visser, J. M. Huijbregtse, J. H. Rector, B. Dam, and R. Griessen, Phys. Rev. Lett. **83**, 2054 (1999).
[9] R. Surdeanu, R. J. Wijngaarden, B. Dam, J. Rector, R. Griessen, C. Rossel, Z. F. Ren, and J. H. Wang, Phys. Rev. B **58**, 12 467 (1998)
[10] S. He, G. L. M. K. S. Kahanda, and P-Z. Wong, Phys. Rev. Lett. **69**, 3731 (1992).
[11] J. Maunuksela, M. Myllys, O.-P. Kähkönen, J. Timonen, N. Provatas, M. J. Alava, and T. Ala-Nissila, Phys. Rev. Lett. **79**, 1515 (1997).
[12] Romualdo Pastor-Satorras, Phys. Rev. E **56**, 5284 (1997).
[13] C. M. Aegerter, R. Günther, and R. J. Wijngaarden, Phys. Rev. E **67**, 051306 (2003).
[14] C. M. Aegerter, K. A. Lörincz , M. S. Welling, and R. J. Wijngaarden, Phys. Rev. Lett. **92**, 058702 (2004) .
[15] Kinga A. Lörincz, and Rinke J. Wijngaarden Phys. Rev. E **76**, 040301(R) (2007).
[16] D. V. Denisov, Y. Y. Villanueva, K. A. Lörincz, S. May, and R. J. Wijngaarden, Phys. Rev. E **85**, 051309 (2012).
[17] A.-L. Barabási and H. E. Stanley, in *Fractal Concepts in Surface Growth* (Cambridge University Press, Cambridge, U.K., 1995).
[18] Mehran Kardar, Giorgio Parisi, and Yi-Cheng Zhang, Phys. Rev. Lett. **56**, 889 (1986).
[19] Luís A. Nunes Amaral, Albert-László Barabási, and H. Eugene Stanley, Phys. Rev. Lett. **73**, 62 (1994).
[20] Luís A. Nunes Amaral, Albert-László Barabási, Hernán A. Makse, and H. Eugene Stanley, Phys. Rev. E **52**, 4087 (1995).
[21] Albert-László Barabási and Tamás Vicsek, Phys. Rev. A **44**, 2370 (1991).
[22] Albert-László Barabási, Roch Bourbonnais, Mogens Jensen, János Kertész, Tamás Vicsek, and Yi-Cheng Zhang, Phys. Rev. A **45**, R6951 (1992).
[23] Stéphane Santucci, Knut Jørgen Måløy, Arnaud Delaplace, Joachim Mathiesen, Alex Hansen, Jan Øistein Haavig Bakke, Jean Schmittbuhl, Loïc Vanel, and Purusattam Ray, Phys. Rev. E **75**, 016104 (2007)
[24] Hans-Karl Janssen, Olaf Stenull, Phys. Rev. E **75**, 020801(R) (2007).
[25] Viktoria Blavatska and Wolfhard Janke, Physics Procedia **3**, Issue 3, 1431–1435 (2010).
[26] Hans-Karl Janssen, Olaf Stenull, Phys. Rev. E **85**, 011123 (2012).
[27] Heiko Leschhorn and Lei-Han Tang, Phys. Rev. E **49**, 1238 (1994).
[28] Maya Paczuski, Sergei Maslov, and Per Bak, Phys. Rev. E **53**, 414 (1996).
[29] S.V. Buldyrev, A.-L. Barabási, F. Caserta, S. Havlin, H.E. Stanley, and T. Vicsek, Phys. Rev. A **45**, R8313 (1992).
[30] V.K. Vlasko-Vlasov, U. Welp, V. Metlushko, and G.W. Crabtree, Phys. Rev. B **69**, 140504(R) (2004).
[31] M.S. Welling, C.M. Aegerter, R.J. Westerwaal, S. Enache, R.J. Wijngaarden, Physica (Amsterdam) C **406**, 100 (2004).
[32] M.S. Welling, R.J. Westerwaal, W. Lohstroh, R.J.Wijngaarden, Physica (Amsterdam) C **411**, 11 (2004).
[33] Igor S. Aranson, A. Gurevich, Marco S. Welling, Rinke J. Wijngaarden, Vitalli K. Vlasko-Vlasov, Valerii M. Vinokur, Ulrich Welp, Phys. Rev. Lett. **94**, 037002, (2005).
[34] J. Guyonnet, E. Agoritsas, S. Bustingorry, T. Giamarchi, P. Paruch, Phys. Rev. Lett. **109**, 147601 (2012).
[35] S. Demirdiş, C. J. van der Beek, Y. Fasano, N. R. Cejas Bolecek, H. Pastoriza, D. Colson, and F. Rullier-Albenque, Phys. Rev. B **84**, 094517 (2011).
[36] F. Rullier-Albenque, D. Colson, A. Forget, and H. Alloul, Phys. Rev. Lett. **103**, 057001 (2009).
[37] L. A. Dorosinskĭi, M. V. Indenbom, V. I. Nikitenko, Yu.A. Ossip'yan, A. A. Polyanskii, and V. K. Vlasko-Vlasov, Physica (Amsterdam) C **203**, 149 (1992).
[38] M. Uehara, C. J. van der Beek, J. Gattacceca, V. A. Skidanov, and Y. Quesnel, Geochem. Geophys. Geosyst. **11**, Q05Y09 (2010); doi:10.1029/2009GC002653.
[39] Y. Fasano and M. Menghini, Supercond. Sci. Technol. **21** 023001 (2008).
[40] B. Duplantier, Phys. Rev. Lett. **82**, 880 (1999).
[41] J. Gilchrist and C.J. van der Beek, Physica (Amsterdam) C **231**, 147 (1994).

[42] Kevin E. Bassler and Maya Paczuski, Phys. Rev. Lett. **81**, 3761 (1998).
[43] Kevin E. Bassler, Maya Paczuski, and George F. Reiter, Phys. Rev. Lett. **83**, 3956 (1999).
[44] This material can be reached as EPAPS document No. E-PRLTAO-94-002506 via the EPAPS homepage (ftp://ftp.aip.org/epaps/phys_rev_lett/E-PRLTAO-94-002506/)